ELSEVIER
Earth and Planetary Science Letters 120 (1993) 473–485
EPSL

Emerald dating through $^{40}Ar/^{39}Ar$ step-heating and laser spot analysis of syngenetic phlogopite

A. Cheilletz [a], G. Féraud [b], G. Giuliani [a,c], G. Ruffet [b]

[a] Centre de Recherches Pétrographiques et Géochimiques et Ecole Nationale Supérieure de Géologie, 15 rue Notre Dame des Pauvres, BP 20, 54501, Vandoeuvre-lès-Nancy, France
[b] Institut de Géodynamique, URA CNRS 1279, Université de Nice-Sophia Antipolis, Parc Valrose, 06034 Nice Cedex, France
[c] ORSTOM, Département TOA, UR 1H, 213 rue La Fayette, 75480 Paris, France

(Received November 6, 1993; revised and accepted September 20, 1993)

Abstract

Emerald, occurring in K-metasomatic rocks developed at the contact of the Carnaíba leucogranite with serpentinite (Bahia State, Brazil), has been dated using an original $^{40}Ar/^{39}Ar$ procedure. It combines step heating and spot fusion experiments on two types of phlogopite crystals: (1) bulk samples and individual grains extracted from the enclosing K-metasomatic host rocks; and (2) syngenetic solid inclusions precipitated along growing zones of the emerald host crystals. The second procedure uses in situ laser probe experiments on rock sections. In spite of the huge amounts of excess ^{40}Ar detected in adjacent emerald, we could measure reliable ages of 1951 ± 8 Ma and 1934 ± 8 Ma for the Trecho Velho and Braulia occurrences, respectively. Spot fusion data had higher discrepancy than the step heating data, but minute crystals of phlogopite included in emeralds bearing excess argon do not reveal excess argon. A muscovite belonging to the same granite hydrothermal complex gave a plateau age of 1976 ± 8 Ma, which may correspond to a higher closure temperature of the K–Ar system during the cooling of the whole pluton and associated hydrothermal halo.

These accurate measurements lead to the following conclusions: (1) direct emerald dating is possible; (2) in spite of a polyphase history during the Transamazonian orogenesis (2 Ga), combined step heating and spot fusion experiments give a better precision for granite-related emerald mineralization than the scattered ages obtained by Rb–Sr and K–Ar methods; (3) the late-Transamazonian tectonothermal retrograde event which probably caused the dispersion of previous Rb–Sr and K–Ar data is not revealed by our procedure; (4) the emerald mineralization and K-metamorphism appear to be linked with the thermal history of the leucogranite; (5) in addition to its use in polyphase crustal domains, accurate $^{40}Ar/^{39}Ar$ dating is of major interest in the field of metallogenic models, even, for instance, for mineralizations characterized by disturbed isotopic systems, which record effects as excess argon.

1. Introduction

Emerald is a green–blue variety of beryl ($Be_3Al_2Si_6O_{18}$), which results from the substitution of chromium for aluminium in the crystal structure. Beryl is the most common mineralogical expression of beryllium, which is considered to be an incompatible element, concentrated during the final stages of granitic and pegmatitic evolutions. Chromium, in contrast, is a typical compatible element, mantle derived, and concen-

[PT]

SSDI 0012-821X(93)E0175-J

trated in ultramafic bodies. Exceptional geological conditions are needed, therefore, to bring together these two elements within the emerald crystal structure, which explains the scarcity of this valuable gem. Geological environments propitious to such juxtaposition are suture zones, granite/greenstone terrains and metamorphosed shales [1]. The Brazilian deposits from Bahia state [2] are good examples of such a process: emeralds are found in K-metasomatized rocks associated with leucogranites and pegmatites intruding serpentinite bodies. The metasomatic rocks are believed to represent the channels of fluid–rock interaction between pegmatitic veins and serpentinites [3,4]. Emerald mineralization therefore appears to be a good witness of granitic emplacement in Archean–Early Proterozoic cratons during continental collisions. However, the polyphase tectonothermal history of such crustal domains caused the frequent resetting of isotopic systems [5,6]. Direct and precise dating of emerald might contribute to a better understanding of the interaction between highly differentiated granite and basement rock during continental accretion.

Natural emerald can contain measurable quantities of Rb. Therefore, the Rb–Sr method was first used for direct emerald dating of the Brazilian deposits (Socoto-Bahia State, Brazil), [7]. These first Rb–Sr determinations, although yielding age ranges compatible with the Transamazonian orogeny (2 Ga), show high discrepancies between model ages of contemporaneous K-metasomatite phlogopite (1814 Ma) and emerald (1180 Ma).

Direct K–Ar dating of beryl and its emerald variety appears difficult due to large amounts of excess argon, which occupies, along with other volatiles (H_20), inert gases (He) and alkali ions (Li, Na, K, Rb and Cs), the hexagonal channels defined by the six-membered silica tetrahedron ring. Values of 82–99% excess argon relative to radiogenic argon have been reported [8,9]. Therefore, the only promising way for precise emerald dating remains, at the moment, the indirect dating of host rocks or K-bearing mineral inclusions which reflect their paragenesis and are very often present in natural emeralds [10,11].

In situ laser probe $^{40}Ar/^{39}Ar$ experiments on minute syngenetic solid inclusions in emerald, combined with $^{40}Ar/^{39}Ar$ step heating on bulk samples and single grains from the host rock, can be carried out on the $^{40}Ar/^{39}Ar$ device of the University of Nice, France [12,13]. This method was attempted on the Carnaíba deposit from Brazil (Bahia sate), which produces emeralds with minute phlogopite grains precipitated along the growing zones of the gems. Phlogopite also represents the main gangue mineral of the host rock, thus allowing comparative $^{40}Ar/^{39}Ar$ dating. This approach requires that the dated minerals are: (1) really co-genetic (this will be discussed in detail in this paper); and (2) completely free from excess argon. Due to the close spatial association of the high excess argon-bearing emeralds and the dated phlogopite hydrous inclusions, we anticipated that some excess argon should also affect the latter. Our results invalidate this statement.

2. Regional geology

The Carnaíba granite and its related emerald deposits belong to the Transamazonian (2 Ga) leucogranites plutons of the Jacobina-Contendas Mirante belt [14–16], which form an elongated structure over 500 km long in the eastern part of the Archaean and lower Proterozoic São Francisco craton (Bahia State, Brazil). The Carnaíba granite is a small, circular (4 km in diameter), homogeneous and fine grained, two-mica leucogranite [17] emplaced within a dome structure of the Jacobina lower Proterozoic formations, which overthrusts the Archaean basement from east to west (Fig. 1). The Jacobina series are composed of thick metaquartzite units, metaconglomerates, mica schists, banded iron formations and intercalated, thin meta-ultrabasic slices (100–300 m thick) bearing stratabound chromium deposits, which have been retromorphosed into serpentinites (Fig. 1). The serpentinite layers are cross-cut by the intrusive granitic pluton or occur as enclaves in the top of the roof-pendant.

The genesis of the Carnaíba-type emerald deposit appears to be well constrained [4,18,19]:

emerald is found in the contact metamorphic rocks of the granite aureole (Fig. 1), within a dense swarm of pegmatites crosscutting the serpentinite slices. The development of emeralds results from a metasomatic process. This is due to the infiltration of hydrothermal fluids throughout both the pegmatites and serpentinites which lead to chemical exchanges, such as, for example: (1) the desilicification and albitization of pegmatites; (2) the biotitization of serpentinites, which resulted in the development of monomineralic mica zones, the so-called K-metasomatites or phlogopitites; and (3) the deposition of emerald and accessory molybdenite and scheelite, within the K-metasomatites or less frequently the albitized pegmatites. During the metasomatic exchanges, the chromium, substituted within the lattice of beryl and giving it its valuable colour, was extracted from the serpentinites. The emerald occurrences were then cross-cut by quartz–molybdenite–muscovite–yellow beryl veins generated during a late hydrothermal phase in the general emerald depositional event.

Later, a barren tectonothermal overprinting, characterized by folding, boudinage, crenulation and a weak chloritization of biotite, affected the granite and the emerald-bearing K-metasomatites. This retromorphic event is attributed to the ultimate tectonic pulses of the Transamazonian orogenesis, since this part of the Saõ Francisco craton is free of tectonothermal events of Brasiliano age (0.6–0.5 Ga) [14,15].

The polyphase geological history of the Carnaíba area probably explains the wide dispersion of radiometric data obtained on granites and related K-metasomatites. A Rb–Sr isochron age at 1883 ± 87Ma [16] has been proposed for the Carnaíba granite, whereas the associated K-metasomatites yield an age of 1869 ± 28 Ma [3]. Muscovites and biotites from the Carnaíba granite yield K–Ar isochron ages of 1980 ± 30 Ma and 1890 ± 32 Ma, respectively [20], whereas the K-metasomatites gave an age of 1958 ± 20 [20]. Such a wide range of ages, determined on muscovite and biotite from the granite and associated contact-metamorphosed surrounding rocks, appear to be probably due to the late Transamazonian tectonothermal overprint, which partly disturbed the original Rb–Sr and K–Ar radiogenic systems, and thus gives scattered ages.

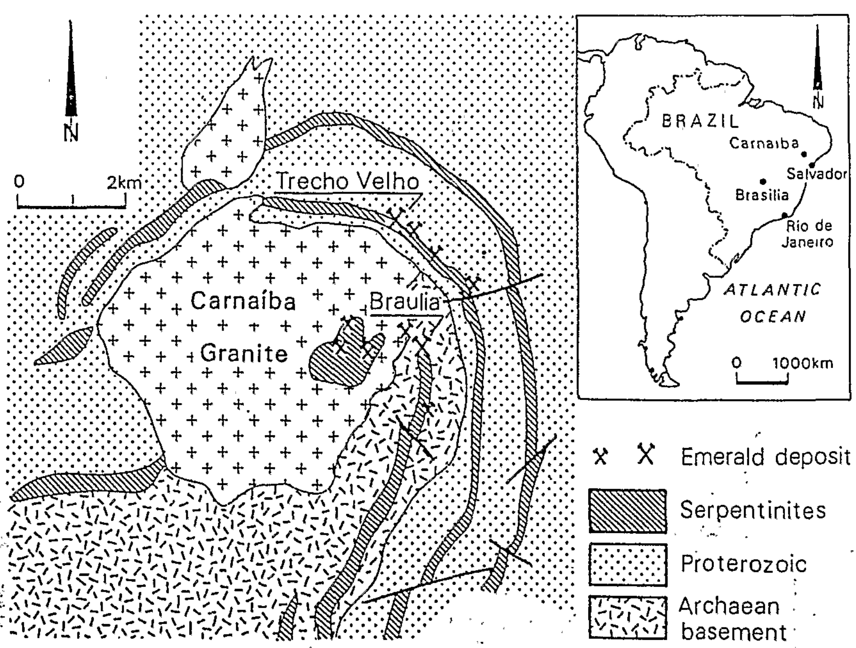

Fig. 1. Geological sketch map of the Carnaíba granite and emerald mining dictrict.

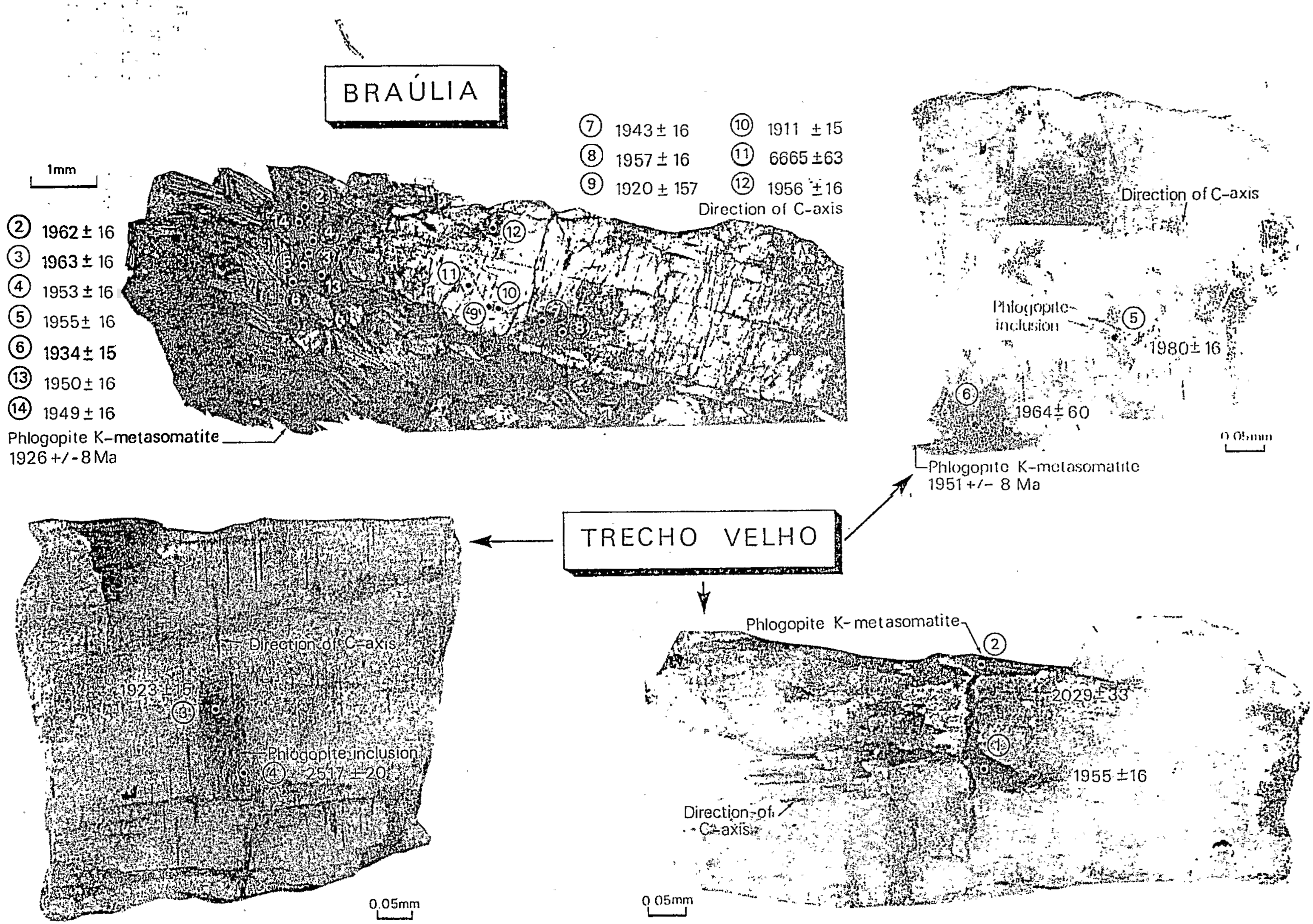

Fig. 2. Location and $^{40}Ar/^{39}Ar$ ages of the laser spot-fusion analysis on the slab samples from Braúlia (BaFl2-II-1) and Trecho Velho (TVFl 6).

It therefore appears necessary to constrain the age of the metasomatic halo and the emerald mineralization accompanying the Carnaíba granite intrusion more precisely. This would allow further valuable comparisons with other leucogranites emplaced within the Jacobina-Contendas Mirante belt [16,20–22], and better knowledge of the Transamazonian orogenesis. Such a goal is made possible by the use of the $^{40}Ar/^{39}Ar$ method which needs fewer samples for analysis than the Rb–Sr or K–Ar techniques, and individual biotite grains or a few grains of ultra-pure unchloritized biotite can be used. The shape of the resulting $^{40}Ar/^{39}Ar$ step-heating spectrum can also be used to validate plateau ages.

3. Sample description

The present study has been carried out using samples of emeralds, K-metasomatites and molybdenite- and muscovite-bearing quartz veins selected in the Trecho Velho and Braúlia prospecting pits (Fig. 1). Two different emerald-bearing ores were studied: Sample TVFl 6 (Trecho Velho) consists of emerald and its K-metasomatite host rock included in metasomatized serpentinites. The K-metasomatite is coarse grained and composed of phlogopite (2 cm long), apatite and minor quartz. Sample Ba FL2-II-1 (Braúlia) belongs to an albitized pegmatite vein showing irregular phlogopite pockets and/or veinlets 1-10 cm in length. In both cases, emerald contains syngenetic phlogopite inclusions (Fig. 2).

The muscovite Ba 102 belongs to a molybdenite–yellow beryl–quartz vein which cross-cuts the emerald-bearing K-metasomatites in the Braúlia deposit.

Phlogopite and muscovite crystals analyzed by the induction and laser step-heating techniques were carefully separated by hand picking. Electron microprobe data and the analytical proce-

Table 1
Microprobe and chemical analysis of muscovite, phlogopite and emerald from the Carnaíba emerald deposit

	Muscovite BA102	Phlogopite					Emerald CATV
		BAFL2-II-1 [1]	TVFl6 [1]	TVFl6 [2]	TVFl6 [2]		
SiO_2	47.27	39.75	41.60	42.52	42.04	SiO_2	64.52
TiO_2	0.13	0.28	0.33	0.26	0.28	TiO_2	< 0.01
Al_2O_3	30.32	17.55	14.28	14.39	14.09	Al_2O_3	16.80
MgO	3.35	13.47	20.04	19.71	19.59	MgO	1.18
CaO	0.02	0.00	0.00	0.00	0.00	CaO	0.25
MnO	0.01	0.53	0.23	0.30	0.28	MnO	< 0.01
FeO	3.40	12.67	7.52	7.39	8.09	Fe_2O_3	0.57
Na_2O	0.33	0.16	0.31	0.30	0.27	Na_2O	1.20
K_2O	10.78	9.85	9.36	9.44	9.62	K_2O	0.038
Rb_2O	0.23	0.36	0.28	0.35	0.53	Rb_2O	0.0038
H_2O	3.80	2.17	1.83	1.94	1.90	H_2O	2.42
F	1.37	3.97	4.85	4.70	4.74	BeO	13.26
O = F	−0.58	−1.67	−2.04	−1.98	−1.99	Li	0.0684
Total	100.43	99.09	98.59	99.32	99.44	Cs	0.1045
						V	0.0068
Fe + Mn/Fe + Mn + Mg	36.38	35.48	17.86	17.99	19.35	Cr	0.0480
						Zn	0.0050
						Total	100.47

Microprobe analyses (Muscovite and phlogopite) were performed at the University of Nancy 1, Service Commun d'Analyses. Analytical conditions: acceleration voltage, 15 kV; sample current 6–8 nA, silicate crystals as standards, and ZAF correction procedure. Chemical analysis of emerald is from CRPG, wet chemical analysis using 500 mg of sample.

[1] Phlogopite outside emerald.

[2] Phlogopite inside emerald.

Table 2
$^{40}Ar/^{39}Ar$ analytical data

	Atmospheric Contamination (%)	^{39}Ar (%)	$^{37}Ar_{Ca}/^{39}Ar_K$	$^{40}Ar^*/^{39}Ar_K$	Apparent age (Ma)	Error ($\pm 1\sigma$)
Bulk sample induction furnace analysis Sample BaFl2-II-1 Analysis M266						
Temperature (°C)						
520	87.468	0.197	9.48E − 03	67.915	1694.09	38.608
540	76.776	0.115	9.01E − 03	66.497	1671	19.8286
610	67.673	0.407	5.19E − 03	54.44	1461.76	10.9801
630	46.666	2.894	2.6E − 03	78.617	1859.41	9.4081
675	17.018	9.013	3.1E − 03	82.886	1921.35	7.0609
690	4.7168	12.23	5.1E − 04	84.126	1938.94	5.1959
700	2.0858	10.16	4.5E − 04	84.557	1945.02	4.8814
710	1.206	8.043	4.7E − 04	84.534	1944.7	4.1493
720	0.77409	5.276	2.9E − 04	84.277	1941.08	3.1374
725	0.46711	7.138	4.4E − 04	84.465	1943.73	3.5623
740	0.82397	2.354	1.02E − 03	84.456	1943.6	2.8065
745	2.6162	1.202	4.44E − 03	84.498	1944.19	9.9779
770	2.9182	1.219	1.77E − 03	84.224	1940.33	2.8574
800	1.2129	2.334	6.6E − 04	84.203	1940.03	2.5976
830	0.9248	3.939	3.6E − 04	84.391	1942.68	3.3901
860	1.0485	6.707	5.7E − 04	84.44	1943.37	3.8855
880	0.8306	6.332	0	84.349	1942.09	3.5737
900	0.78027	6.852	5.5E − 04	84.386	1942.61	3.705
920	0.85805	4.376	6.5E − 04	84.15	1939.28	4.5757
930	0.98145	3.006	9E − 04	84.113	1938.76	3.2796
940	1.5421	1.448	8.9E − 04	83.684	1932.69	3.0547
970	1.4639	1.817	8.5E − 04	83.816	1934.56	2.7393
1020	1.5848	2.367	5.7E − 04	84.155	1939.35	3.5244
1120	6.4475	0.558	2.98E − 03	84.325	1941.75	3.9131
1450	94.157	0.013	0.54505	126.49	2455.69	226.013
Integrated age = 1934.9 ± 1.3						
Single grain laser analysis Sample BaFl2-II-1 Analysis M303						
Steps						
1	92.038	0.085	3.1213	63.392	1619.4	897.076
2	79.547	0.174	0.44137	48.212	1343.36	114.204
3	40.386	0.91	0	65.276	1650.89	29.1406
4	7.1525	5.388	0.03894	81.708	1904.47	7.0244
5	2.8355	6.882	0.05601	82.939	1922.1	7.5578
6	2.1416	7.453	0.06822	82.899	1921.53	5.5671
7	2.0656	8.054	0.06772	83.207	1925.92	4.652
8	1.8661	8.408	0.02312	83.092	1924.28	4.5586
9	1.8731	8.803	0.04864	83.012	1923.14	4.8972
10	1.5355	10.78	0.04356	83.127	1924.78	4.584
11	0.88	9.009	0.0333	83.573	1931.12	5.9352
12	0.9773	7.546	0.02702	83.31	1927.38	5.6662
13	0.8422	7.767	0.05084	83.157	1925.21	7.2701
14	0.56418	4.667	0.03584	83.7	1932.92	7.77
15	0.84569	3.419	0.04914	83.272	1926.84	7.2785
16	0.49996	3.484	0.05365	83.31	1927.38	7.5495
17	0.74242	5.138	0.07541	83.569	1931.06	7.8758
18	1.5055	1.06	7.03E − 03	82.831	1920.56	34.6233
19	1.5865	0.973	0.0495	83.942	1936.34	24.4761
Integrated age = 1921.1 ± 1.8						

Table 2 (continued)

	Atmospheric Contamination (%)	^{39}Ar (%)	$^{37}Ar_{Ca}/^{39}Ar_K$	$^{40}Ar^*/^{39}Ar_K$	Apparent age (Ma)	Error ($\pm 1\sigma$)
Single grain laser analysis Sample TVFl6 Analysis M313						
Steps						
1	22.837	0.201	0	78.75	1861.37	50.6804
2	8.5619	0.146	0	71.442	1750.26	92.6925
3	2.2656	0.697	0	78.489	1857.52	19.0478
4	1.0407	5.185	0.04209	84.453	1943.56	11.3319
5	0.36906	12.39	0.05041	85.492	1958.14	6.1478
6	0.31878	10.15	0.05913	84.853	1949.18	17.8912
7	0.11144	8.223	0.04586	85.752	1961.77	4.7663
8	0.18775	5.886	0.08464	85.4	1956.85	6.6829
9	0.21291	5.145	0.07166	85.272	1955.06	6.7487
10	0.16812	7.04	0.0461	85.449	1957.53	5.6099
11	0.23469	7.351	0.06389	85.004	1951.3	8.1114
12	0.33796	6.571	0.07522	84.679	1946.74	10.0641
13	0.28793	6.398	0.0736	85.035	1951.74	9.0711
14	0.2827	5.549	0.07646	84.727	1947.41	7.5119
15	0.36971	5.292	0.09275	84.661	1946.49	4.9999
16	0.17917	6.639	0.04579	84.463	1943.7	8.7487
17	0.10057	3.78	0.06863	84.325	1941.75	9.4591
18	7.9768	3.347	0.05847	84.598	1945.6	18.2172
Integrated age = 1950.4 ± 2.7						
Bulk sample induction furnace analysis Sample Ba102a Analysis M267						
Temperature (°C)						
500	78.216	0.095	0.03853	50.111	1380.3	78.4596
570	43.707	0.193	0.01531	59.305	1549.13	18.3736
650	41.369	0.121	0.07099	76.5	1827.89	66.9549
710	20.045	0.525	0.01368	87.071	1980.07	5.9197
750	15.36	0.656	0.0142	80.487	1886.8	5.2121
790	19.16	0.58	0.04975	75.231	1808.72	7.0541
840	4.8988	2.539	3E − 03	88.186	1995.4	3.2394
880	1.3372	14.68	6.9E − 04	87.438	1985.13	3.114
900	0.33905	8.433	1.15E − 03	86.901	1977.72	2.4787
920	0.26234	15.55	7E − 04	86.778	1976.02	3.1453
925	0.19816	15.18	8.9E − 04	86.758	1975.74	6.6579
930	0.22361	8.468	3.9E − 04	86.844	1976.93	3.0125
935	0.32884	4.825	1.33E − 03	86.636	1974.05	3.3142
940	0.30377	4.245	2.37E − 03	86.632	1974	2.4035
950	0.37281	3.501	9.9E − 04	86.795	1976.25	4.1377
960	0.42321	1.795	5.05E − 03	87.296	1983.17	2.8245
970	0.37733	2.878	2.43E − 03	86.691	1974.81	2.0074
980	0.45328	2.521	2.88E − 03	86.751	1975.64	3.2367
990	0.32083	3.315	1.47E − 03	86.876	1977.37	2.4998
1010	0.37761	3.178	1.25E − 03	86.786	1976.13	2.4835
1060	0.31732	4.419	1.97E − 03	86.866	1977.24	3.0898
1160	1.94	2.029	3.58E − 03	87.041	1979.65	10.2773
1450	51.143	0.254	0.07438	86.598	1973.53	140.407
Integrated age = 1975.0 ± 1.4						

dure for micas are listed in Table 1. The muscovite Ba102 contains 3.4% FeO and 3.4% MgO, placing it in the phengite series. Phlogopite presents two distinct compositions: the crystals included within the TVFl 6 emerald or in the K-metasomatite enclosing rock display identical compositions, having 18% annite (Fe + Mn/Fe + Mn + Mg ratio; Table 1), whereas the Ba FL2-II-1 K-metasomatite shows a higher annite content (36%, Table 1). This annite content difference reflects the host rock composition: the Braúlia K-metasomatite was developed from a pegmatite, whereas the Trecho Velho K-metasomatite derives from a serpentinite which originally had a lower Fe/Mg ratio [3], which buffers the metasomatic process forming biotites with a higher Mg content.

ICPAE spectrometry and chemical analysis of an emerald crystal from Trecho Velho (CATV) are presented in Table 1. It shows the usual enrichment in Cr, Fe and V of Brazilian emeralds [2]. These emeralds are also characterized by a relatively high Cs (0.1%) and Li (0.07%) and a low K_2O content (0.038%).

4. Experimental procedure

Laser spot fusion procedures were performed on 1 mm thick slabs of emerald-bearing K-metasomatites obtained by microsawing parallel to the c axis of the emerald (Fig. 2); one sample from Braúlia and three samples from Trecho Velho were investigated (Fig. 2).

The laser-probe device and procedure of the University of Nice (France) are described elsewhere [12,13]. The samples were irradiated in the Osiris reactor (Saclay, France) with a total integrated flux of 10^{19} n/cm^2 and rotated during irradiation. The flux monitor was the hornblende MMhb-1 [23]. Analytical data are presented in Figs. 2 and 3 and Tables 2 and 3; age calculations were made using isotope correction procedures, standard plateau age definition [13,24], recommended decay constants [25] and are given with 1σ standard error estimates. The error on the irradiation factor, J, is not included in the calculation of individual age errors in the step heating experiments. For the plateau age calculation, we included the error due to the flux, which is ±0.4% on each level of irradiation where the standard was analyzed. Owing to a higher contribution of this error bar relative to the other factors, we obtained a constant error bar of 8 Ma on the

Table 3
$^{40}Ar/^{39}Ar$ laser spot fusion analytical data

Spot No.	Atmospheric contamination (%)	^{39}Ar cc STP ($\times 10^{-12}$)	$^{37}Ar_{Ca}/^{39}Ar_K$	$^{40}Ar^*/^{39}Ar_K$	Age (Ma)	Error $\pm 1\sigma$
Spot laser flogopite BaF12-II-1						
2	0.19	48.7	0.05	85.79	1962	±14
3	0.18	128.8	0.05	85.87	1963	±16
4	0.41	48.3	0.05	85.10	1952	±16
5	0.15	31.7	0.05	85.25	1955	±16
6	0.09	67.2	0.09	83.79	1934	±15
7	1.84	121.4	0.05	84.42	1943	±16
8	5.63	55.5	0.09	85.41	1957	±16
9	2.02	1.7	2.06	82.80	1920	±157
10	1.32	12.0	0.04	82.15	1911	±15
11	3.86	5.2	1.45	1710.00	6665	±63
12	0.56	10.5	0.07	85.33	1956	±16
13	1.61	7.9	0.05	84.89	1950	±16
14	0.50	49.4	0.04	84.85	1949	±16
Spot laser phlogopite TV FL6						
1	3.66	26.6	0.03	85.29	1955	±16
2	37.22	6.0	0.00	90.63	2029	±33
3	6.62	7.9	0.00	82.98	1923	±15
4	1.38	27.9	0.14	132.38	2517	±20
5	3.02	115.5	0.09	87.05	1980	±16
6	41.56	5.2	0.00	85.88	1964	±60

plateau ages for all samples. Because of the flux gradient along the vertical axis of the irradiation can, and the large dimension of the rock slab, we estimate the error bars on laser spot ages at ±0.8%. This explains the errors of ±15–16 Ma on most of the laser spot ages (for which the error due to the flux gradient is dominant) and the same minimum error bars on the calculated means.

5. $^{40}Ar/^{39}Ar$ dating results

Step heating experiments: Bulk sample induction furnace analyses were performed on muscovite Ba 102 and K-metasomatite phlogopite BaFl2-II-1 samples. Single grains of K-metasomatite phlogopite BaFl2-II-1 and TVFl 6 were also analyzed through the laser step-heating procedure. The isotopic ratio and apparent ages are reported in Tables 2 and 3 and the corresponding age spectra in Fig. 3. All samples display remarkable flat age spectra, yielding plateau ages at 1976 ± 8 Ma for muscovite Ba 102 (bulk sample), 1951 ± 8 Ma for phlogopite TVFL 6 (single grain), 1942 ± 8 Ma (bulk sample) and 1926 ± 8 Ma (single grain) for phlogopite Ba FL2-II-1 (Fig. 3). These plateau ages were calculated with more than 90% of the total ^{39}Ar released (except for bulk sample BaFl2-II-1: 81%) and are, in this

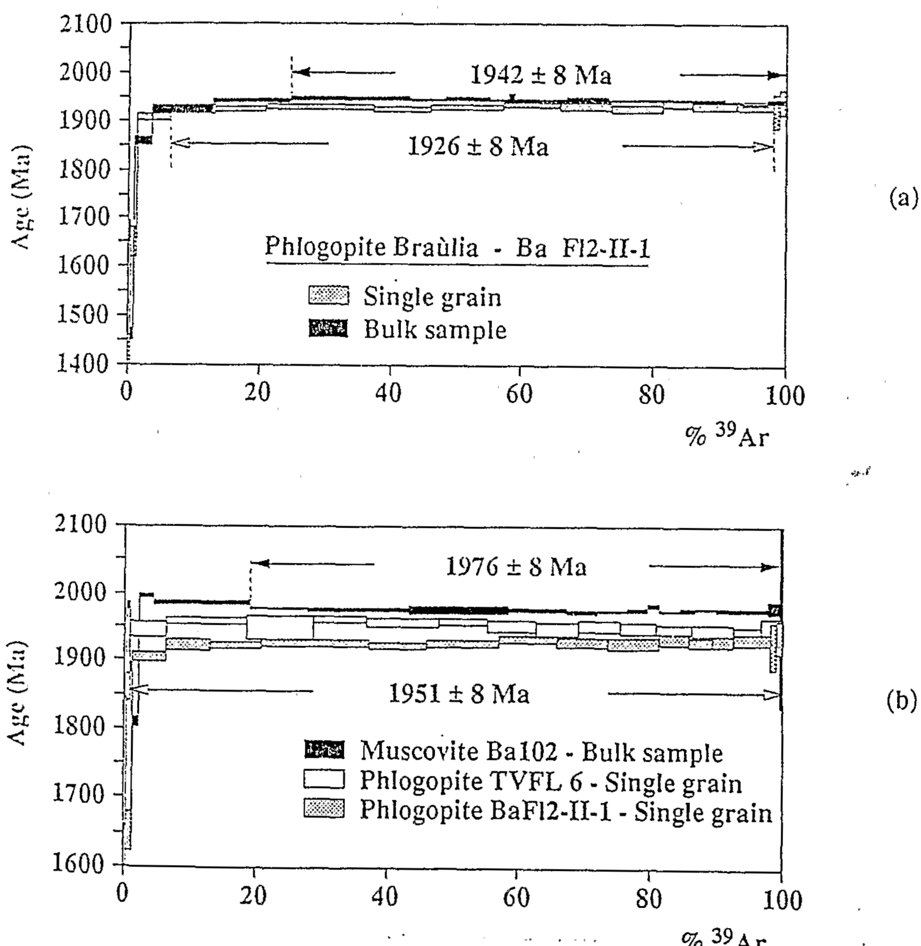

Fig. 3. (a) $^{40}Ar/^{39}Ar$ spectra of the Braúlia phlogopite. (b) Comparison of $^{40}Ar/^{39}Ar$ spectra of the Braúlia (BaFl2-II-1) muscovite (Ba 102) and phlogopite (BaFl2-II-1) and the Trecho Velho (TVFl 6) phlogopite.

way, within 0.5% of the integrated calculated ages (Table 2).

Spot fusion experiments: Spot fusion experiments were performed on phlogopite crystals from K-metasomatite enclosing rock, on phlogopite inclusions within the emerald crystals and on emerald. The age results and the location of the spots are presented in Fig. 2 and isotopic data in Table 3. For the Braúlia sample BaFl2-II-1 (Fig. 2), a good concordance appears (spot 10 excepted) between the analyses performed on phlogopite inclusions and those on the K-metasomatite: the mean age for the largest inclusion (1 mm long; spots 7 and 8) is 1948 ± 16 Ma. One spot (no. 12) on a small inclusion (0.1 mm long) yields 1956 ± 16 Ma. The most precise age on a smaller solid inclusion (0.2 mm long; spot 10) gives a younger age of 1911 ± 15 Ma. For the three spots 7, 8 and 12, the weighted mean age is 1949 ± 16 Ma. The seven analyses (spots 2–6, 13 and 14) performed on one phlogopite crystal from the enclosing rock (Fig. 2) give ages ranging from 1934 ± 15 Ma and 1963 ± 18 Ma, and a weighted mean age of 1956 ± 16 Ma.

Evidence for excess argon is clearly provided by the high $^{40}Ar^{*}/^{39}Ar_{K}$ ratio (1710; Table 3) obtained from the Braúlia emerald crystal spot (no 11; Table 3) which gives an unrealistic age. The higher $^{37}Ar_{Ca}/^{39}Ar_{K}$ ratio (1.45) linked with this result should also be noted.

Three spots (3, 4 and 5) were measured on phlogopite included in the Trecho Velho emerald crystals, and three spots (1, 2 and 6) on the K-metasomatite enclosing rock; one of them (1) is situated on a phlogopite fracture zone within an emerald crystal. The ages measured on spots 1–3 and 5 in K-metasomatites and inclusions are concordant (using a 2σ confidence level) with the plateau age at 1951 ± 8 Ma; whereas spot 4 displayed a clearly older age of 2517 ± 20 Ma.

6. Discussion of ages

6.1 Phlogopite ages

For the phlogopite BaFl2-II-1, a concordance within the error bars is found (Fig. 3) between the plateau ages displayed by the bulk sample and single grain (1942 ± 8 Ma and 1926 ± 8 Ma, respectively) of the metasomatite, the laser spot fusion ages obtained on the metasomatites (weighted mean age: 1956 ± 16 Ma; spots 2–6, 13 and 14), and the inclusion in the emerald (weighted mean age: 1949 ± 16 Ma; spots 7, 8 and 12), one small inclusion age excepted (spot 10: 1911 ± 15 Ma). No excess argon could be detected even on small phlogopite inclusions. The bulk sample age spectrum shows a regular increase in ages at low temperatures (Fig. 3), which appears more clearly than for single grains. This may be related to the higher degree of alteration in the bulk sample.

The step-heating experiments performed on one single grain of sample TVFl 6 displayed a plateau age of 1951 ± 8 Ma, which is not concordant with the previous results at the 1σ confidence level (Table 2). The laser spot ages on both the metasomatites and the phlogopite inclusions are more scattered (from 1923 ± 15 to 2517 ± 20 Ma). These variations seem to be correlated with variable $^{37}Ar_{Ca}/^{39}Ar_{K}$ ratios (from 0.0 to 0.14) and atmospheric contamination. If we reject the two results (spots 2 and 6) affected by the highest atmospheric contaminations (37% and 42%, respectively), we observe a positive correlation between the ages obtained and the measured $^{37}Ar_{Ca}/^{39}Ar_{K}$ ratios (Table 3). This may indicate that the higher ages are the results of a contamination of the phlogopite by emerald (the $^{37}Ar_{Ca}/^{39}Ar_{K}$ ratio measured on pure emerald is 1.45; spot 11 of BaFl2-II-1). This interpretation is supported by the fact that the laser beam was parallel to the cleavage planes of micas in the TVFl 6 slab and perpendicular in the case of BaFl2-II-1. During the laser heating procedure of the spot fusion experiment, we could observe, in some cases, a large opening of the cleavage planes of the phlogopites, allowing a deeper penetration of the laser beam, which could warm up the host emerald or hidden inclusions. It should be noticed that Ca-bearing inclusions; that is, apatite and plagioclase, are common in the K-metasomatite paragenesis of the Carnaíba deposit [18], which may play the same contaminant role as emerald if they contain excess argon.

The ages obtained for both samples by step heating were more precise and clustered than the spot fusion analyses. This was due to: (1) a better knowledge of the flux gradient; and (2) a higher purity of the mineral phases analyzed in the separate minerals than in the slab plate. We therefore propose ages of 1934 ± 8 Ma (weighted mean of the two step heating experiments) and 1951 ± 8 Ma for the phlogopites BaFl2-II-1 and TVFl 6, respectively.

6.2 Muscovite age

The muscovite Ba 102 yields a plateau age of 1976 ± 8 Ma (Fig. 3), which is clearly older (even at the 2σ confidence level) than the plateau age obtained on the phlogopite BaFl2-II-1. In spite of a small difference in age (2%), this result is in apparent contradiction with field relationships; muscovite belongs to the quartz–molybdenite veins crosscutting the emerald-bearing K-metasomatites. This aspect is discussed in the following section.

7. Thermochronology of the Carnaíba pluton and related hydrothermal processes

The $^{40}Ar/^{39}Ar$ ages obtained on phlogopites from the two sites of Trecho Velho (1951 ± 8 Ma) and Braúlia (1934 ± 8 Ma) are concordant using a 2σ confidence level (± 16 Ma), whereas the muscovite Ba 102 displayed a plateau age at 1976 ± 8 Ma, which is clearly older than the ages obtained on the Braúlia phlogopites. Clear geological and geochemical evidence shows that granite emplacement, the formation of emerald contained in K-metasomatites, and later hydrothermal quartz–molybdenite vein development are nearly contemporaneous. This is shown by the fact that: (1) the quartz–molybdenite vein system presents the same bulk geochemical spectrum (Mo–W–Be) as the granite–metasomatite complex; (2) fluid inclusion study of emerald-bearing metasomatites yield homogenization temperatures of about 400°C, identical to the temperatures measured for the quartz–molybdenite veins [Giuliani, pers. commun., 1992].

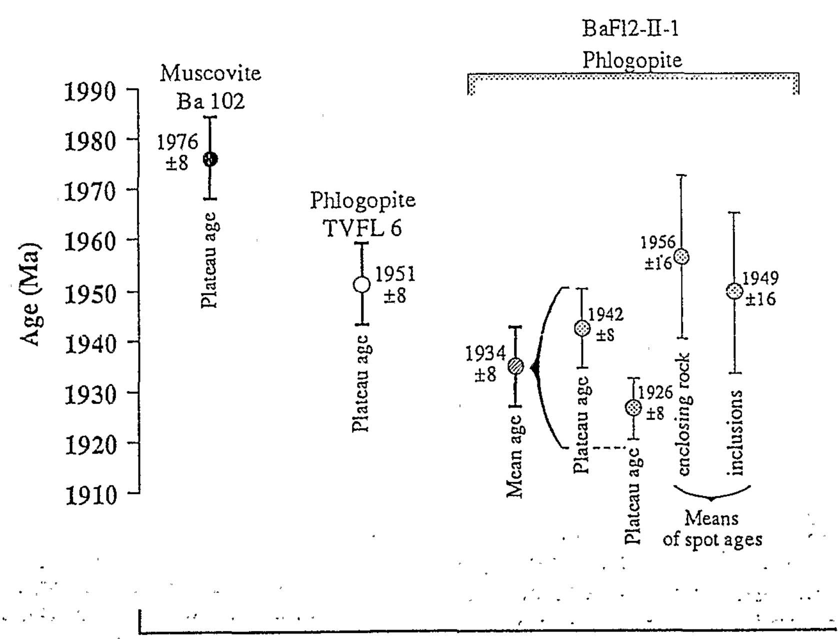

Fig. 4. Total variation range of $^{40}Ar/^{39}Ar$ ages from the Braúlia and Trecho Velho emerald deposits considering "plateau" and "spot" ages.

If we consider as reliable the ages of 1976 ± 8, 1951 ± 8 (plateau ages) and 1934 ± 8 Ma (the means of the two plateau ages at 1942 and 1926 Ma) for the muscovite Ba 102, the phlogopite TVFl 6 and Ba Fl2-II-1, respectively (Fig. 4), we may tentatively explain the age differences as representing the successive closure of the K–Ar system of the minerals, rather than crystallisation order, during cooling of the whole granite–hydrothermal system, in spite of the low difference of the three ages (the maximum difference is 2%). The closure temperature possibly decreases from muscovite Ba 102, to phlogopite TVFl 6 (annite content 18%), then to phlogopite BaFl2-II-1 (annite content 36%). The inverse correlation between the closure temperature of biotites and the annite content (related to the Fe/Mg ratio) has been proposed from hydrothermal experiments [26].

8. Conclusions

The dating of minerals bearing excess argon is possible using $^{40}Ar/^{39}Ar$ laser spot and step heating analyses of syngenetic phlogopite occurring as inclusions within emerald crystals and their K-metasomatic gangue. Minute phlogopite crystals included in beryls bearing excess argon do not show any excess argon. For two emerald deposits located at the contact of the Carnaíba leucogranite, Bahia State, Brazil, the results show phlogopite ages of 1951 ± 8 and 1934 ± 8 Ma, which are concordant at the 2σ confidence level.

The higher discrepancy of spot fusion data compared with step heating data may result from: (1) the deeper penetration of the laser beam when it is parallel to the cleavage plane of the micas, which may release argon from hidden extra-mineral phases; and (2) flux gradients during irradiation, which is not easily monitored on relatively large (> 5 mm) polished slab samples.

The entire results, for both syngenetic phlogopites of emerald deposits and muscovite belonging to a quartz–molybdenite vein crosscutting the emeralds, are concordant with the fast cooling of the whole granite-hydrothermal system.

This work helps to establish the formation age of the Carnaíba granite-related emerald deposits as being within the Transamazonian (2 Ga) orogenesis.

Acknowledgements

Field and laboratory studies were funded by grants from the ATP PIRSEM "Métallogénie des métaux de haute technologie" no 91N80/0095 to A.C. and G.F., from ORSTOM, Dept. TOA UR 1H to G.G. and from CRPG-CNRS équipe "Géochimie des Gaz et ses applications" to A.C. and G.G.J. Gerbaut and L. Frappier typed the tables and Y. Leistreit and C. Moreau carefully drafted the illustrations. CRPG contribution no. 995.

References

[1] A.H. Kazmi and L.W. Snee, Emeralds of Pakistan, Geology, Gemology and Genesis, 269 pp., Van Nostrand Rheinhold, New York, 1989.
[2] T. Eidt and D. Schwarz, Die Smaragde von Carnaíba, Bahia, Brasilien; vorkommen und charakteristika, Z. Dtsch. Gemmol. Ges. 36, 3–4, 1987.
[3] L. Rudowski, Pétrologie et géochimie des granites transamazoniens de Campo Formoso et Carnaíba (Bahia, Brésil), et des phlogopitites à émeraudes associées, 300 pp., Ph.D. Thesis, Univ. Paris VI, 1989.
[4] G. Giuliani, L.J.H.D. Silva and P. Couto, Origin of emerald deposits of Brazil, Miner. Deposita 25, 57–64, 1990.
[5] B.B. Britos Neves, U.G. Cordani and J.R.F. Torquato, Evoluçao geocronologica do Pré-cambriano do Estado da Bahia, in: Geologia e Recursos Minerais do Estado da Bahia, Salvador, Vol. 3, H.A.V. Inda and F.B.V Duarte, eds., pp. 1–80, S.M.E., Salvador, 1980.
[6] M. Cuney, P. Sabaté, P. Vidal, M.M. Marinho and H. Conceiçao, The 2 Ga peraluminous magmatism of the Jacobina-Contendas Mirante belt (Bahia) Brazil: Major and trace-element geochemistry and metallogenic potential, J. Volcanol. Geotherm. Res. 44, 123–141, 1990.
[7] Ph. Vidal, B. Lasnier and J.P. Poirot, Determination of the age and origin of emeralds using rubidium–strontium analysis, J. Gemmnol. 23 (4), 198–200, 1992.
[8] P.E. Damon and J.L. Kulp, Excess helium and argon in beryl and other minerals, Am. Mineral. 43, 433, 1958.
[9] F. Leutwein and G. Kaplan, Quelques recherches sur l'aptitude de certains cristaux de néoformation à capturer de l'argon radiogénique, C.R. Acad. Sci. 257 (II), 1315–1317, 1963.

[10] J. Sinkankas, Beryl, 225 pp., P.R. Read, ed., Butterworths, London, 1986.
[11] D. Schwarz, Esmeraldas, Inclusoes em Gemas, 439 pp., Impresa Univ. Ouro Preto, Ouro Preto, 1987.
[12] S. Scaillet, G. Féraud, Y. Lagabrielle, M. Ballèvre and G. Ruffet, $^{40}Ar/^{39}Ar$ laser-probe dating by step heating and spot fusion of phengites from the Dora Maira nappe of the western Alps, Italy, Geology 18, 741–744, 1990.
[13] G. Ruffet, G. Féraud and M. Amouric, Comparison of $^{40}Ar/^{39}Ar$ conventional and laser dating of biotites from the North Trégor Batholith, Geochim. Cosmochim. Acta 55, 1675–1688, 1991.
[14] U.G. Cordani and B.B. Brito Neves, Geocronólogia do Precambriano, in: Texto explicativo para o mapa geológico do Estado da Bahia, escala 1:1000000, H.A.V. Inda and J.F. Barbosa, eds., pp. 32–49, S.M.E. Salvador, 1982.
[15] J.M. Bertrand and E.F. Jardím de Sa, Where are the Eburnian–Transamazonian collisonial belts?, Can. J. Earth Sci. 27, 1382–1393, 1990.
[16] P. Sabaté, M.M. Marinho, P. Vidal and M. Caen Vachette, The 2 Ga peraluminous magmatism of the Jacobina-Contendas Mirante belt (Bahia, Brazil): geologic and isotopic constraints on the sources, Chem Geol. 83, 325–338, 1990.
[17] L. Rudowski and M. Fonteilles, Existence de deux séries évolutives distinctes dans les granites peralumineux de Campo Formoso, et leurs relations avec le granite de Carnaíba et les minéralisations à émeraudes (Serra de Jacobina, Bahia, Brésil). C.R. Acad. Sci. 307 (II), 935–940, 1988.
[18] L. Rudowski, G. Giuliani and P. Sabaté, Les phlogopitites à émeraude au voisinage des granites de Campo Formoso et Carnaíba (Bahia, Brésil): un exemple de minéralisation protérozoique à Be, Mo et W dans des ultrabasites métasomatisées, C.R. Acad. Sci. 301 (II), 1129–1134, 1987.
[19] P.A. Couto, E.A. Da Silva and R. Lima, Garimpos de esmeralde de Carnaiba e Socoto, Bahia, in: Principais Depositos Minerais do Brazil, Vol. IV, Parte A, pp. 259–269, DNPM-CPRM, Brasilia, 1991.
[20] G. Giuliani, J.L. Zimmermann, A. Cheilletz and R. Montigny, Comparison of K–Ar and $^{40}Ar/^{39}Ar$ ages on granites and on emerald-bearing metasomatites from Campo Formoso and Carnaíba, Bahia, Brazil, Terra Cognita 3 (1), 500, 1991.
[21] J.R. Torquato, M.A.F. Tanner de Oliveira and R.L. Bartels, Idade radiométrica do granito de Campo Formoso, Bahia. Uma idade minima para o Grupo Jacobina, Rev. Bras. Geochím. 8, 171–179, 1978.
[22] L. Turpin, P. Maruejol and M. Cuney, Comparative U–Pb, Rb–Sr and Sm–Nd chronology of granitic basement, hydrothermal albitites and uranium mineralization (Lagoa Real, South Bahia, Brazil), Contrib. Mineral. Petrol. 98, 139–147, 1988.
[23] S.D. Samson and E.C. Alexander Jr., Calibration of the interlaboratory $^{40}Ar/^{39}Ar$ dating standard, MMhb-1, Chem. Geol. Isotope Geosci. Sect. 66, 27–34, 1987.
[24] G. Féraud, D. York, C. Mével, G. Cornen, C.M. Hall and J.M. Auzende, Additional ^{39}Ar–^{40}Ar dating of the basement and the alkaline volcanism of Gorringe bank (Atlantic Ocean), Earth Planet. Sci. Lett. 79, 255–269, 1986.
[25] R. Steiger and E. Jaëger, Subcommission on geochronology: Convention on the use of decay constants in geo- and cosmochronology, Earth Planet. Sci. Lett. 36, 359–362, 1977.
[26] T.M. Harrisson, I. Duncan and I. McDougall, Diffusion of ^{40}Ar in biotite: Temperature, pressure and compositional effects, Geochim. Cosmochim. Acta 49, 2461–2468, 1985.

REPRINTED FROM:

EARTH AND PLANETARY SCIENCE LETTERS

Earth and Planetary Science Letters 120 (1993) 473–485

Emerald dating through $^{40}Ar/^{39}Ar$ step-heating and laser spot analysis of syngenetic phlogopite

A. Cheilletz [a], G. Féraud [b], G. Giuliani [a,c], G. Ruffet [b]

[a] *Centre de Recherches Pétrographiques et Géochimiques et Ecole Nationale Supérieure de Géologie, 15 rue Notre Dame des Pauvres, BP 20, 54501, Vandoeuvre-lès-Nancy, France*

[b] *Institut de Géodynamique, URA CNRS 1279, Université de Nice-Sophia Antipolis, Parc Valrose, 06034 Nice Cedex, France*

[c] *ORSTOM, Département TOA, UR 1H, 213 rue La Fayette, 75480 Paris, France*

(Received November 6, 1993; revised and accepted September 20, 1993)

ELSEVIER

Amsterdam—London—New York—Tokyo